Numerical analysis of sound insulation performance of double-layer wall with vibration absorbers using FDTD method

Shuo-Yen LIN[1]; Shinichi SAKAMOTO[2]

[1] Graduate School, the University of Tokyo

[2] Institute of Industrial Science, the University of Tokyo

ABSTRACT

For investigating the detail effects of the vibration absorbers in the cavity of the double-layer wall (DLW), a vibro-acoustic numerical model was developed and the behavior of the system was simulated by the finite-difference time-domain method (FDTD method). By comparing the results for various cases, the mechanism of the vibration absorber in the DLW and the effects of the location side and the distribution patterns of the vibration absorbers on the sound insulation performance of the DLW had been confirmed. The deterioration of the sound insulation performance of the DLW due to the mass-air-mass resonance can be improved by the vibration control. In spite of that, setting the vibration absorbers in the cavity causes the movement of the original resonance to the other frequency band and the occurrence of the second resonance. The problems can be dissolved by the sound absorption of the damping material in the vibration absorber. In the investigation, the changes of the sound insulation performance are low correlated with the conditions of the different location side and distribution patterns of the vibration absorbers in the DLW.

Keywords: Sound insulation, Vibration absorber, Double-layer wall, FDTD method
I-INCE Classification of Subjects Number(s): 33, 47.4

1. INTRODUCTION

Applying the vibration absorbers assembled of the vibration mass and the damping material in the double-layer wall (DLW) to improve the deterioration at mass-air-mass resonance frequency band had been confirmed in scale model experiments (1, 2). The sound insulation performance was raised by the works of the vibration absorbers due to vibration control and sound absorption.

The other reason for the improvement at the original resonance frequency band may be due to the vibration absorbers in the cavity taking some space as the obstacles to avoid the occurrence of the mass-air mass resonance. Therefore the improvement of the sound insulation performance is due to the vibration control, sound absorption and the obstacles factor.

However, it is difficult to verify the mechanism of the vibration absorbers in the cavity only by one-dimension analysis and scale model experiments (2, 3). Thus, two-dimensional numerical analysis by the finite-difference time-domain method (FDTD method) was proceeded for investigating the detail mechanism of the vibration absorbers. Moreover, we verified the effects of the location side of the vibration absorbers and that of the distribution patterns of the vibration absorbers on the sound insulation performance of the double-layer wall.

2. NUMERICAL MODEL

2.1 Model Explanation

A two-dimension model of the double-layer wall shown in Figure 1(a) is constituted by two walls with length L (m), thickness h (m), and distance d (m). The double-layer wall divides the air into three parts which are the source side, the cavity and the transmission side. The other two models indicate the vibration absorber assembled by damping material and vibration mass located on the

[1] sylin@iis.u-tokyo.ac.jp
[2] sakamo@iis.u-tokyo.ac.jp

wall 1 (Source side) and wall 2 (Transmission side) respectively as shown in Figure 1(b) and 1(c). In the three figures, p_i, p_r, and p_t, are the incident sound pressure (N/m^2), the reflecting sound pressure (N/m^2) and the transmitting sound pressure (N/m^2) , respectively. p_1, p_2, p_3, and p_4, are the sound pressures (N/m^2) on the surface of the walls and vibration mass in the cavity. In addition, the x direction is defined as vertical and y axis is defined as horizontal in the figures.

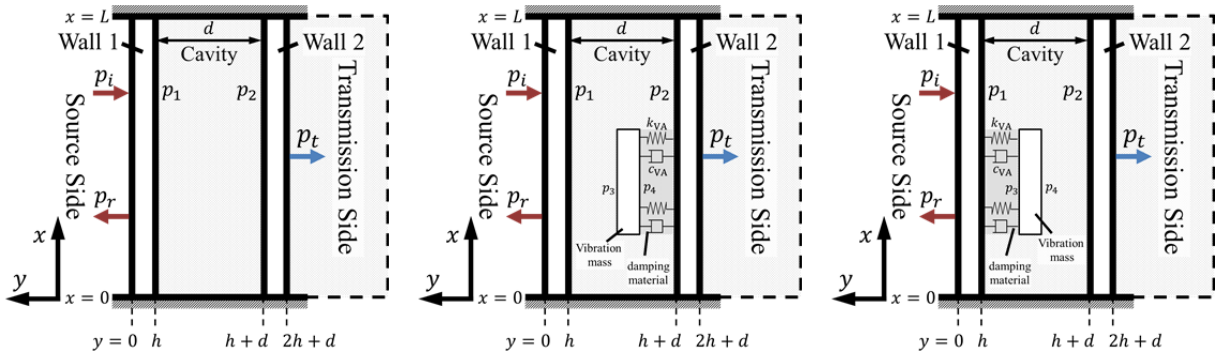

(a) DLW without the vibration absorber

(b) DLW with the vibration absorber on the transmission side

(c) DLW with the vibration absorber on the source side

Figure 1 – The diagram of the double-layer wall in two-dimension.

2.2 Government Equations

In this investigation, the walls are so thin that the Euler-Bernoulli beam theory is adopted (4). Therefore the behavior of the two walls made of the same material can be described as

$$EI\left(1+\xi\frac{\partial}{\partial t}\right)\frac{\partial^4 u_j}{\partial x^4}+m\frac{\partial^2 u_j}{\partial t^2}+m\mu\frac{\partial u_j}{\partial t}=q_j, \tag{1}$$

where E is the young's modulus (N/m^2), I is the second moment of area (m^4), ξ is the internal damping (s), μ is the external damping (1/s), and m is the area density (kg/m^2) of the walls. Here u_j and q_j denote the displacement (m) and the external pressure of the j_{th} wall respectively.

Eq. (1) denotes the government equation of the part of the wall not coupled with the vibration absorber. When the wall is coupled with the vibration absorber as shown in Figure 1(b) and 1(c), the government equation of the part of the wall becomes

$$EI\left(1+\xi\frac{\partial}{\partial t}\right)\frac{\partial^4 u_j}{\partial x^4}+m\frac{\partial^2 u_j}{\partial t^2}+m\mu\frac{\partial u_j}{\partial t}+c_{\mathrm{VA}}\left(\frac{\partial u_j}{\partial t}-\frac{\partial u_{\mathrm{VA}}}{\partial t}\right)+k_{\mathrm{VA}}\left(u_j-u_{\mathrm{VA}}\right)=q_j, \tag{2}$$

and the government equation of the vibration mass can be expressed as

$$E_{\mathrm{VA}}I_{\mathrm{VA}}\left(1+\xi_{\mathrm{VA}}\frac{\partial}{\partial t}\right)\frac{\partial^4 u_{\mathrm{VA}}}{\partial x^4}+m_{\mathrm{VA}}\frac{\partial^2 u_{\mathrm{VA}}}{\partial t^2}+m_{\mathrm{VA}}\mu_{\mathrm{VA}}\frac{\partial u_{\mathrm{VA}}}{\partial t}+c_{\mathrm{VA}}\left(\frac{\partial u_{\mathrm{VA}}}{\partial t}-\frac{\partial u_j}{\partial t}\right)+k_{\mathrm{VA}}\left(u_{\mathrm{VA}}-u_j\right)=q_3, \tag{3}$$

where c_{VA} is the damping coefficient (N-s/m^3) and k_{VA} is the spring constant per unit area (N/m^3) of the damping material. The other parameters with subscript VA denote the properties and displacement of the vibration mass. Additionally, q_3 is the external pressure applied on the vibration mass.

The external pressures q_1, q_2 and q_3 in Eqs. (1)-(3) are correlated with the sound pressures p_i, p_r, p_t, p_1, p_2, p_3, and p_4 as

$$q_1=p_i+p_r-p_1;\ \ q_2=p_2-p_t;\ \ q_3=p_3-p_4. \tag{4}$$

The ends of the each wall terminate fully clamped boundary conditions which can be described as follows:

$$u_j=0;\ \frac{\partial u_j}{\partial x}=0. \tag{5}$$

The vibration mass is supported by the rectilinear springs and dampers thus the boundary condition can be described as

$$E_{\mathrm{VA}}I_{\mathrm{VA}}\left(1+\xi_{\mathrm{VA}}\frac{\partial}{\partial t}\right)\frac{\partial^3 u_{\mathrm{VA}}}{\partial x^3}+m_{\mathrm{VA}}\mu_{\mathrm{VA}}\frac{\partial u_{\mathrm{VA}}}{\partial t}+c_{\mathrm{VA}}\left(\frac{\partial u_{\mathrm{VA}}}{\partial t}-\frac{\partial u_j}{\partial t}\right)+k_{\mathrm{VA}}(u_{\mathrm{VA}}-u_j)=0, \tag{6}$$

$$\frac{\partial^2 u_{\mathrm{VA}}}{\partial x^2}=0. \tag{7}$$

The sound propagation in the cavity and transmission side can be described by using Euler's equations with airflow resistance and continuity equation as follows:

$$\frac{\partial v_x}{\partial t}+\frac{1}{\rho}\frac{\partial p}{\partial x}=\frac{r}{\rho}v_x;\ \ \frac{\partial v_y}{\partial t}+\frac{1}{\rho}\frac{\partial p}{\partial y}=\frac{r}{\rho}v_y, \tag{8}$$

$$\frac{\partial p}{\partial t}+\rho c^2\left(\frac{\partial v_x}{\partial x}+\frac{\partial v_y}{\partial y}\right)=0, \tag{9}$$

where p is the sound pressure (N/m^2), v_x, v_y are the particle velocities (m/s) of the air, ρ is the density (kg/m^3) of the air, c is the sound speed (m/s) in the air, and r is the airflow resistance (N-s/m^4). In Eq. (9), the airflow resistance is to simulate the sound absorption of the damping material in the cavity.

At the top and the bottom in the cavity, the rigid boundaries are assumed. Around the transmission side, 2$^{\mathrm{nd}}$ Higdon's absorbing boundary conditions are applied to simulate the perfectly absorbing boundary conditions.

For the numerical analysis by the FDTD method, we converted the partial differential equation to difference equations and set the proper coupling conditions for the vibro-acoustic analysis explained in next two sections.

2.3 Difference Equations

Rewriting the partial differential equations Eqs. (1)-(3) to the difference equations, the displacements of the walls and vibration mass are calculate by the difference equations as follows:

[1] the wall without the vibration absorber

$$\begin{aligned}u_{j_i}^{n+1}&=2u_{j_i}^{n}-u_{j_i}^{n-1}+q_j\frac{\Delta t^2}{m}-\mu\Delta t\left(u_{j_i}^{n}-u_{j_i}^{n-1}\right)\\&-\frac{EI}{\Delta x^4}\frac{\Delta t^2}{m}\left[\left(1+\frac{\xi}{\Delta t}\right)\left(u_{j_{i-2}}^{n}-4u_{j_{i-1}}^{n}+6u_{j_i}^{n}-4u_{j_{i+1}}^{n}+u_{j_{i+2}}^{n}\right)-\frac{\xi}{\Delta t}\left(u_{j_{i-2}}^{n-1}-4u_{j_{i-1}}^{n-1}+6u_{j_i}^{n-1}-4u_{j_{i+1}}^{n-1}+u_{j_{i+2}}^{n-1}\right)\right].\end{aligned} \tag{10}$$

[2] the wall with the vibration absorber

$$\begin{aligned}u_{j_i}^{n+1}&=2u_{j_i}^{n}-u_{j_i}^{n-1}+q_j\frac{\Delta t^2}{m}-\mu\Delta t\left(u_{j_i}^{n}-u_{j_i}^{n-1}\right)-\frac{c_{VA}\Delta t}{m}\left[\left(u_{j_i}^{n}-u_{j_i}^{n-1}\right)-\left(u_{VA_i}^{n}-u_{VA_i}^{n-1}\right)\right]-\frac{k_{VA}\Delta t^2}{m}\left(u_{j_i}^{n}-u_{VA_i}^{n}\right)\\&-\frac{EI}{\Delta x^4}\frac{\Delta t^2}{m}\left[\left(1+\frac{\xi}{\Delta t}\right)\left(u_{j_{i-2}}^{n}-4u_{j_{i-1}}^{n}+6u_{j_i}^{n}-4u_{j_{i+1}}^{n}+u_{j_{i+2}}^{n}\right)-\frac{\xi}{\Delta t}\left(u_{j_{i-2}}^{n-1}-4u_{j_{i-1}}^{n-1}+6u_{j_i}^{n-1}-4u_{j_{i+1}}^{n-1}+u_{j_{i+2}}^{n-1}\right)\right].\end{aligned} \tag{11}$$

[3] the vibration mass

$$\begin{aligned}u_{\mathrm{VA}_i}^{n+1}&=2u_{\mathrm{VA}_i}^{n}-u_{\mathrm{VA}_i}^{n-1}+q_3\frac{\Delta t^2}{m_{\mathrm{VA}}}-\mu_{VA}\Delta t\left(u_{\mathrm{VA}_i}^{n}-u_{\mathrm{VA}_i}^{n-1}\right)-\frac{c_{\mathrm{VA}}\Delta t}{m_{\mathrm{VA}}}\left[\left(u_{\mathrm{VA}_i}^{n}-u_{\mathrm{VA}_i}^{n-1}\right)-\left(u_{j_i}^{n}-u_{j_i}^{n-1}\right)\right]-\frac{k_{\mathrm{VA}}\Delta t^2}{m_{\mathrm{VA}}}\left(u_{\mathrm{VA}_i}^{n}-u_{j_i}^{n}\right)\\&-\frac{E_{\mathrm{VA}}I_{\mathrm{VA}}}{\Delta x^4}\frac{\Delta t^2}{m_{\mathrm{VA}}}\left[\left(1+\frac{\xi}{\Delta t}\right)\left(u_{\mathrm{VA}_{i-2}}^{n}-4u_{\mathrm{VA}_{i-1}}^{n}+6u_{\mathrm{VA}_i}^{n}-4u_{\mathrm{VA}_{i+1}}^{n}+u_{VA_{i+2}}^{n}\right)-\frac{\xi}{\Delta t}\left(u_{\mathrm{VA}_{i-2}}^{n-1}-4u_{\mathrm{VA}_{i-1}}^{n-1}+6u_{\mathrm{VA}_i}^{n-1}-4u_{\mathrm{VA}_{i+1}}^{n-1}+u_{\mathrm{VA}_{i+2}}^{n-1}\right)\right].\end{aligned} \tag{12}$$

where i is the space operator with interval Δx in x direction and n is the time operator with interval Δt.

By using the displacements, the the vibration velocities of the j_{th} wall and the vibration mass are obtained by the forward difference as

$$v_{j_i}^{n}=\frac{u_{j_i}^{n+1}-u_{j_i}^{n}}{\Delta t};\ \ v_{\mathrm{VA}_i}^{n}=\frac{u_{\mathrm{VA}_i}^{n+1}-u_{\mathrm{VA}_i}^{n}}{\Delta t}. \tag{13}$$

Eq. (8) and (9) are rewritten to difference equations as follows:

$$\begin{aligned}v_{x_{l,k}}^{n+1}&=\left(1-\frac{r\Delta t}{\rho}\right)v_{x_{l,k}}^{n}+\frac{\Delta t}{\rho\Delta x}\left(p_{l,k}^{n}-p_{l-1,k}^{n}\right),\\v_{y_{l,k}}^{n+1}&=\left(1-\frac{r\Delta t}{\rho}\right)v_{y_{l,k}}^{n}+\frac{\Delta t}{\rho\Delta y}\left(p_{l,k}^{n}-p_{l,k-1}^{n}\right),\end{aligned} \tag{14}$$

$$p_{l,k}^{n+1}=p_{l,k}^{n}+\rho c^2\Delta t\left(\frac{v_{x_{l+1,k}}^{n+1}-v_{x_{l,k}}^{n+1}}{\Delta x}+\frac{v_{y_{l,k+1}}^{n+1}-v_{y_{l,k}}^{n+1}}{\Delta y}\right), \tag{15}$$

where l and k are the space operators with interval Δx, Δy in x and y direction, respectively. n is the time operator with interval Δt.

2.4 Coupling Conditions in FDTD Method

The discretizations at the fluid–solid boundaries of the models mentioned in sec 2.1 are shown in Figure 2. Figure 2(a) shows the fluid–solid boundary between wall 1 and the air. Figure 2(b) shows the fluid–solid boundary between wall 2 and the air. Figure 2(c) shows the fluid–solid boundary between vibration mass and the air. In the three figures, the grid with thick line denotes the solid area and the grid with thin line are the fluid area. The dots are the definition points of the sound pressure in the cavity and transmission side and the arrows mean the particle velocities of the air.

As shown in Figure 2(a), the external pressure q_1 is calculated by the difference of the sound pressure $p_{i_l}^n$, $p_{r_l}^n$, and $p_{l,1}^n$ at two side of the wall 1. The particle velocity $v_{y_{l,1}}^n$ is the same as the vibration velocity $v_{1_i}^n$ obtained by using Eqs. (10), (11) and (13). The similar concepts are applied at the fluid–solid boundaries of the wall 2 and the vibration mass.

As shown in Figure 2(b), the external pressure q_2 is calculated by the difference of the sound pressure $p_{l,8}^n$ and $p_{t_{l,1}}^n$ at two side of the wall 2. The particle velocities $v_{y_{l,9}}^n$ and $v_{ty_{l,1}}^n$ are equivalent to the vibration velocity $v_{2_i}^n$.

Figure 2(c) shows the discretization near the vibration mass. The external pressure q_3 is calculated by the difference of the sound pressure $p_{l,3}^n$ and $p_{l,6}^n$ at the two side of the vibration mass. The particle velocities $v_{y_{l,4}}^n$ and $v_{y_{l,6}}^n$ are both equal to the vibration velocity $v_{\mathrm{VA}_i}^n$. In addition, the movement of the vibration mass is considered in y direction only, so the $v_{\mathrm{VA},x}$, is set to 0 in this investigation.

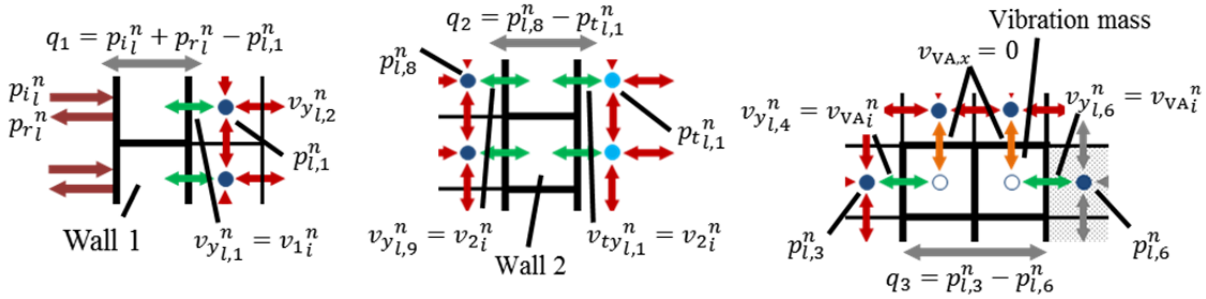

(a) boundaries at wall 1 (b) boundaries at wall 2 (c) boundaries at vibration mass

Figure 2 – The fluid–solid boundaries at two walls and the vibration mass.

On the basis of the equations and the given conditions, the sound insulation performance of the DLW can be expressed by the sound reduction index: R

$$R = 20\log\left|\frac{p_i}{p_t}\right|, \tag{16}$$

where the p_i and p_t are the averaged values for all elements of the walls in the calculation.

3. PROPERTIES MEASUREMENT

3.1 Measurement Instruments

The investigations in numerical analysis simulated a scale model of double-layer wall constructed by plywood (1-3), thus the properties of the plywood were measured to use in the FDTD method.

As mentioned in Sec. 2.2, the young's modulus, internal damping and external damping should be known for the simulation. The properties can be measured by the central exciting method (4). A vibration is given to the specimen and its impedance can be calculated by the feedback signals of the force and velocity. The peaks and dips in the curve of the impedance frequency response of the specimen mean the resonance and anti-resonance. The young's modulus can be calculated by using the resonance frequencies and the loss factor can be obtained by using half-width method.

The instruments of the measurement are shown in Figure 3. The vibration is given by the exciter (B&K Type 4809) to the center of the plywood specimen with its density of 550 (kg/m^3) and dimension of 300 mm (L) x 9 mm (W) x 4 mm (H). The signals of the vibration force and velocity were measured by the impedance head (B&K Type 8001) and passed through the Charge to CCLD Converters (B&K Type 2647A) to the analyzer (B&K 3560B).

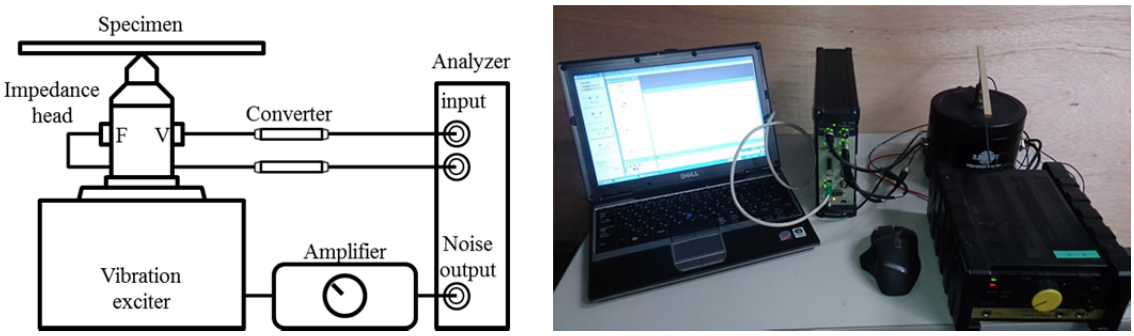

(a) System diagram (b) System picture

Figure 3 – Measurement Instruments

3.2 Results and Analysis

The measured impedance frequency response of the plywood is shown in Figure 4. As the results of the measurement, the resonances occur at 114 Hz, 615 Hz, 1573 Hz, 2093 Hz, and 4439 Hz. The young's modulus of the plywood can be obtained by applying the equation (5) as

$$E = \frac{48\pi^2 l_s^4 \rho_s f_n^2}{h_s^2 \theta_n^4}, \tag{17}$$

where l_s, h_s, and ρ_s are the length, the thickness and the density of the plywood specimen. θ_n is the normalized eigenvalue and f_n is the resonance frequency.

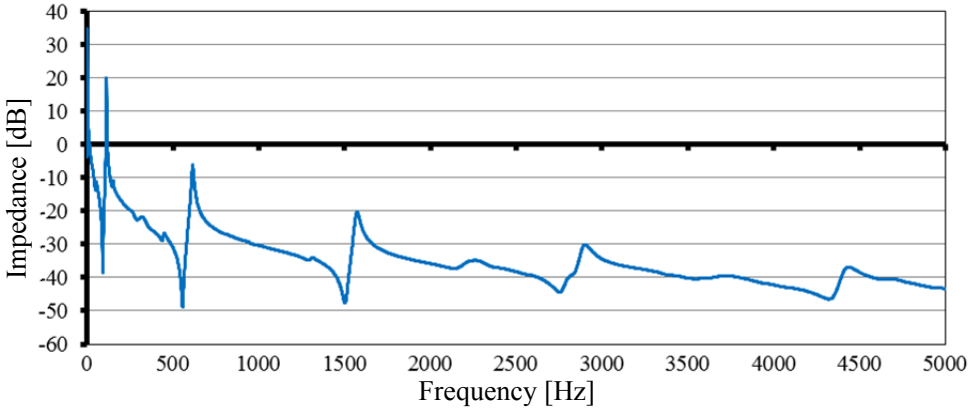

Figure 4 – The impedance frequency response of the plywood

On the basis of Figure 4, the average young's modulus of the plywood was calculated as 3.48 x 10^9 (N/m^2) and the loss factors at the four resonance frequencies were list in Table 1.

Table 1 – The loss factors at the resonance frequencies

Frequency (Hz)	Loss factor
114	0.006156
615	0.017930
1573	0.019231
2093	0.030915
4439	0.037862

By importing Rayleigh damping (4), the loss factor η is the combination of the internal damping ξ and the external damping μ as mentioned in Sec. 2.2 and can be written as

$$\eta = 2\pi f \xi + \frac{\mu}{2\pi f}. \tag{18}$$

Using Eq. (18) to approximate the measurement results of the loss factor as shown in Figure 5, the internal and external damping was probably determined as 1.72 x 10^{-6} (s) and 3.43 (1/s),

respectively.

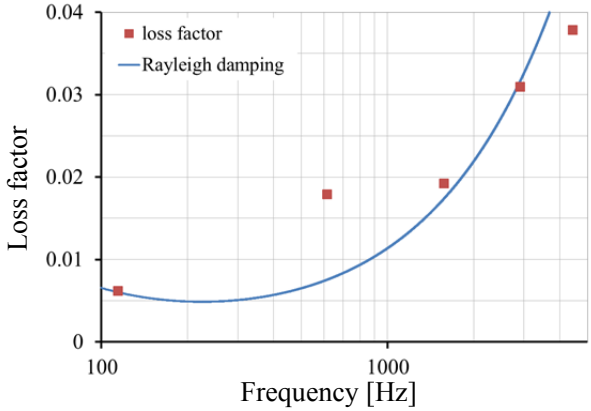

Figure 5 – The loss factor and Rayleigh damping

3.3 Parameters List

The values of the parameters mentioned above for the simulation FDTD analysis are listed in Table 2. In the list, young's modulus and external damping of the vibration absorber are determined in the same way as plywood we measured. In addition, the value of the internal damping as mentioned in Sec. 2.2 is too small and therefore the value can be neglected in the calculation.

Table 2 – The list of the parameters

Symbol	Description	Value	Symbol	Description	Value
E	Young's modulus	3.48×10^{9}	E_{VA}	Young's modulus	3.48×10^{9}
I	Second moment of area	5.33×10^{-9}	I_{VA}	Second moment of area	6.67×10^{-10}
m	Area density	2.2	m_{VA}	Area density	1.72
μ	External damping	3.43	μ_{VA}	External damping	3.43
L	Length	0.8	h_{VA}	Thickness	0.002
h	Thickness	0.004	c_{VA}	Damping coefficient (2)	1.64×10^{3}
d	Distance	0.008	k_{VA}	Spring constant (2)	2.71×10^{7}
ρ	Density of the air	1.2	c	Sound speed in the air	340
Δx	Space interval	10^{-3}	r	Airflow resistance	10^{4}
Δy	Space interval	10^{-3}	Δt	Time interval	1.63×10^{-7}

4. INVESTIGATION AND RESULTS

4.1 The Mechanism of the Vibration Absorber in the Cavity

According to the references (1-3), the vibration absorbers located in the cavity of the DLW provide the vibration control, the sound absorption and the obstacle factor to improve the sound insulation performance of the DLW. The obstacle factor means the vibration absorbers take some space in the cavity and make the air gap ununiform to involve the occurrence of the mass-air mass resonance. The three factors were investigated by comparing five cases as shown in Figure 6. We applied four vibration absorbers with the same size to cover half the area of the wall in the cavity.

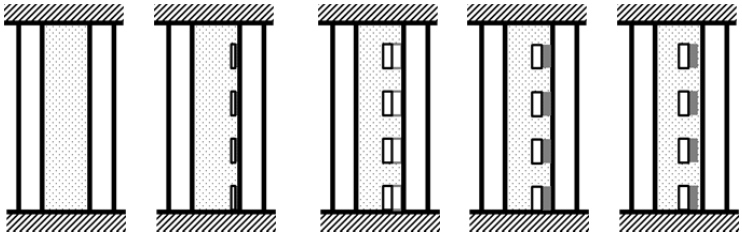

(a) DLW (b) Case1 (c) Case 2 (d) Case 3 (e) Case 4

Figure 6 – Different patterns of the vibration absorbers in DLW.

Figure 6(a) shows a DLW without the vibration absorbers as the reference case. In Figure 6(b), the vibration abosbers are so thin that the sound absorption and the ostacle factor can be neglected.

In this case, only the vibration control by the vibration absorber the works. Figure 6(c) shows the vibration absorbers as the obstacles in the cavity and the damping material without sound absorption. Figure 6(d) shows the general case of the vibration absorbers in the cavity. In this case, three factors were considered. In Figure 6(e), the vibration absorbers are located in the cavity but are not connected to the wall, therefore the vibration control does not work.

The factors considered in each case are listed in the Table 3.

Table 3 – The cases list

	Vibration control	Sound absorption	Obstacles factor
DLW	X	X	X
Case1	O	X	X
Case2	O	X	O
Case3	O	O	O
Case4	X	O	O

The results are shown as Figure 7. The black solid line denotes the sound insulation performance of the DLW. There is an obvious dip at 630 Hz band which means the mass-air-mass resonance as we designed.

For the Case 1 in Figure 7(a), the vibration control provides an obvious improvement of sound insulation performance at 630 Hz band but the sound insulation performance is worse than that of the DLW at 1 kHz due to the movement of the mass-air-mass resonance. The improvement at high frequency bands is caused by the work of the external damping of the vibration mass.

The improvement at 630 Hz band in the Case 2 is close to that in the Case 1 and the mass-air-mass resonances occur at 800 Hz band and 2 kHz band. The occurrence of the other mass-air-mass resonance is caused by a part of the air gap changed by the obstacles.

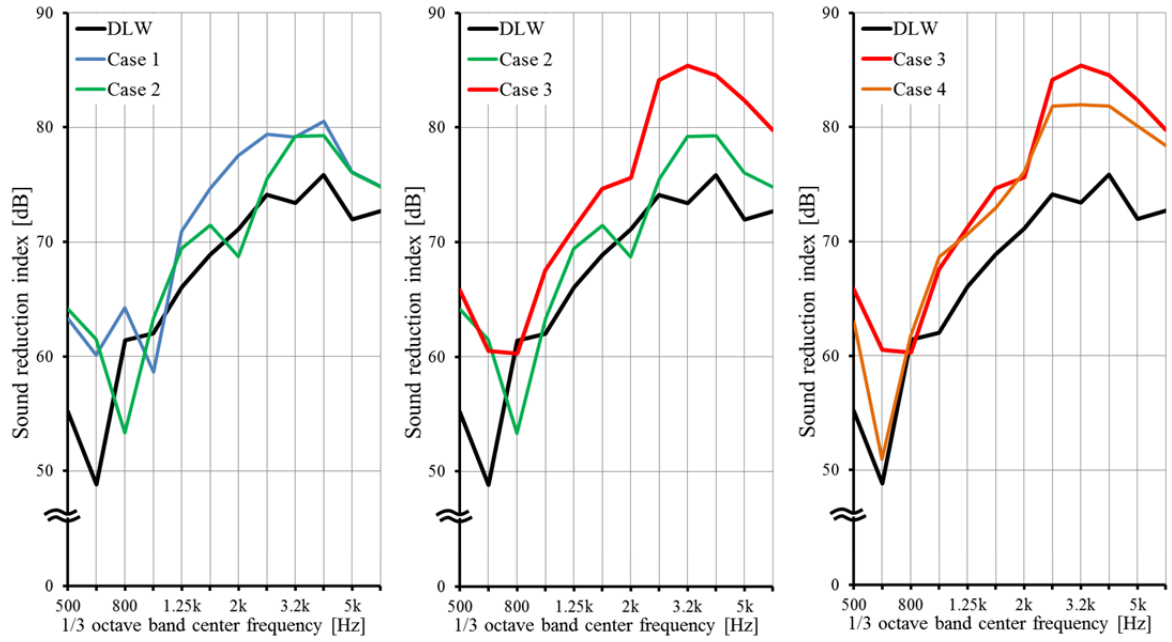

(a) Investigation of the obstacles factor

(b) Investigation of the Sound absorption

(c) Investigation of the Vibration control

Figure 7 – Cases comparison.

Comparing the Case 2 and Case 3 in Figure 7(b), the deterioration of the sound insulation performane due to the resonance at 800 Hz band and 2 kHz band can be compensated by the vibration absorbers with the sound absorption. The sound absorption also provides improvement at the other frequency bands higher than 630 Hz band.

The contrast of the Case 3 and Case 4 in Figure 7(c) denotes the work of the vibration control. In Case 4, the sound insulation performance at 630 Hz band was low and that at the other bands was

close to that of the Case 3. The comparison indicates the improvement of the sound insulation performance at mass-air-mass resonance frequency band is mainly due to the vibration control of the vibration absorbers rather than the other factors. As a result in this section, setting the vibration absorbers in the DLW can control the original resonance frequency band, but it causes the deterioration at the other frequency bands due to the movement of the mass-air-mass resonance and the occurrence of the other resonance. This problem can be dissolved by using the damping material having sound absorption.

4.2 The Effects of Distribution Patterns and Location side of the Vibration Absorbers

To verify the effect of the distribution patterns of the vibration abosrbers in the two-dimension model, the sound insulation performances of the DLW with the vibration abosrbers in four patterns shown in Figure 8(b)-(e) were compared. In Figure 8(b)-(e), the vibration absorbr(s) take half the area of the wall in every pattern.

In our former research, the effect of the location side of the vibration absorbers had been examined by one-dimension model and experiments. The sound insulation performances of the DLW at the mass-air-mass frequency band were the same in two cases of the vibration absorbers put on the souece and transmission sides (3). In this study, more factors were considered by the two dimensional investigation. Figure 9 shows the variations of the vibration absorbers located on the source side as the contrast to Figure 8.

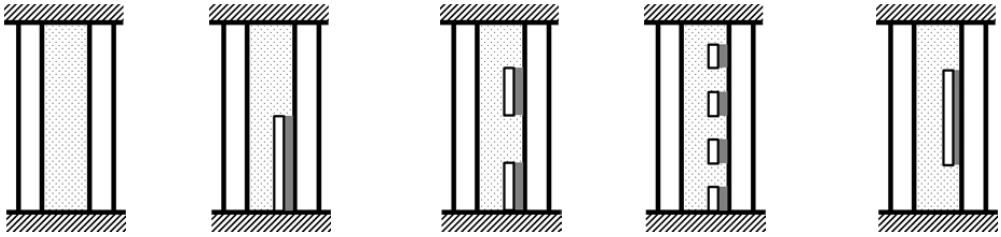

(a) DLW (b) pattern 1, T: 1 absorber at bottom (c) pattern 2, T: 2 absorbers (d) pattern 4, T: 4 absorbers (e) pattern C, T: 1 absorbers at center

Figure 8 – Distribution patterns of the vibration absorbers on the transmission side in DLW.

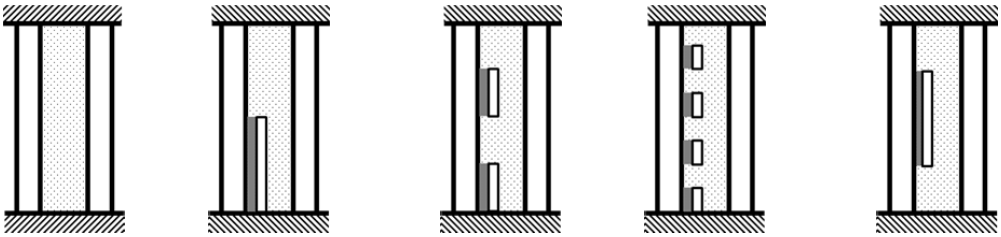

(a) DLW (b) pattern 1, S: 1 absorber at bottom (c) pattern 2, S: 2 absorbers (d) pattern 4, S: 4 absorbers (e) pattern C, S: 1 absorbers at center

Figure 9 – Distribution patterns of the vibration absorbers on the source side in DLW.

Figures 10(a) and 10(b) show the results for the vibration absorbers located on the transmission side and the source side respectively.

From Figures 10(a) and 10(b), the vibration absorbers distributed in all patterns can provide an improvement of sound insulation performance at 630 Hz band due to the vibration control but the mass-air-mass resonances moves to 800 Hz band. To see the other frequency bands, the same level performances can be observed except for 1.6 kHz band. At this frequency band, the other resonance occurs at 1.6 kHz band in pattern 1, pattern 2 and pattern C, and it occurs at 2 kHz in pattern 4.

Additionally, Figure 10(c) shows the comparison of pattern 4, T and pattern 4, S in Figure 8(d) and 9(d). It points out the sound insulation performances are not correlated with the location side of the vibration absorbers in the DLW as the walls are made of the same area density.

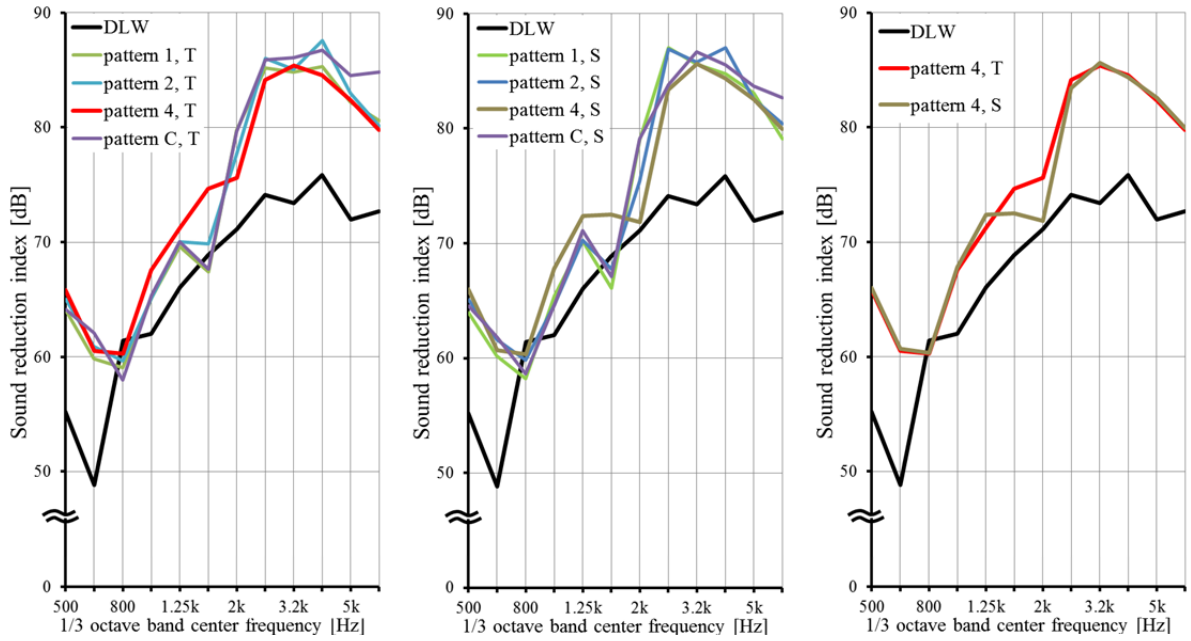

(a) Side T, 4 patterns (b) Side S, 4 patterns (c) patterns, Side S, T

Figure 10 – The comparisons of the cases

(S is the vibration absorber located on the source side and T is on the transmission side.)

5. CONCLUSIONS

The investigations had been confirmed the mechanism of the vibration absorbers in the DLW by numerical analysis. The improvement of the sound insulation performance is owing to three factors which are the vibration control, the sound absorption and the obstacle effect of the vibration absorbers. The deterioration of the sound insulation performance of the DLW due to the mass-air-mass resonance can be improved by the work of the vibration control. But the vibration control and the obstacle effect cause the movement of the mass-air-mass resonance and the occurrence of the other resonance. For the problem, using a damping material with sound absorption is an adopted solution.

The development of the numerical model by FDTD method makes the detail verification of the vibration absorbers in the DLW become possible. Many conditions such as the distribution patterns of the vibration absorber, the different materials for the wall and the vibration absorbers and etc. will be investigated in the future.

ACKNOWLEDGEMENTS

This research was partially supported by the Obayashi Foundation.

REFERENCES

1. Lin SY, Tsujimura S, Yokoyama S, Sakamoto S. Improvement of sound transmission loss of double-layer wall by using vibration absorber. J. Acoust. Soc. Jpn. 2014;35(2);119-121.
2. Lin SY, Tsujimura S, Yokoyama S, Sakamoto S. Improvement of sound insulation performance of double-layer wall by using vibration absorbers. Proc INTER-NOISE 2013; 15-18 September 2013; Innsbruck, Austria 2013. paper 0690.
3. Lin SY, Tsujimura S, Yokoyama S, Sakamoto S. Difference of sound insulation and plate vibration characteristics of the double-layer wall by variation of locations of vibration absorbers. The 2014 Spring Meeting of the Acoustical Society of Japan; 10-12 March 2014; Tokyo, Japan 2014. p. 1157-8.
4. Asakura T, Sakamoto S. Numerical simulation on the sound insulation performance of wall system by vibro-acoustical numerical analysis using FDTD method. Seisan Kenkyu 2009;61(4);793-796.
5. Maymon G. Structural Dynamics and Probabilistic Analysis for Engineers. Burlington, Massachusetts, USA: Butterworth-Heinemann; 2008.